Pressure effects in the itinerant antiferromagnetic metal TiAu

C. T. Wolowiec,[1,2] Y. Fang,[2,3] C. A. McElroy,[1,2,*] J. R. Jeffries,[4] R. L. Stillwell,[4] E. Svanidze,[5,†] J. M. Santiago,[5] E. Morosan,[5] S. T. Weir,[4] Y. K. Vohra,[6] and M. B. Maple[1,2,3,‡]

[1]*Department of Physics, University of California, San Diego, La Jolla, California 92093, USA*
[2]*Center for Advanced Nanoscience, University of California, San Diego, La Jolla, California 92093, USA*
[3]*Materials Science and Engineering Program, University of California, San Diego, La Jolla, California 92093, USA*
[4]*Condensed Matter and Materials Division, Lawrence Livermore National Laboratory, Livermore, California 94550, USA*
[5]*Department of Physics and Astronomy, Rice University, Houston, Texas 77005, USA*
[6]*Department of Physics, University of Alabama at Birmingham, Birmingham, Alabama 35294, USA*

(Received 10 April 2017; published 7 June 2017)

We report the pressure dependence of the Néel temperature T_N up to $P \approx 27$ GPa for the recently discovered itinerant antiferromagnet (IAFM) TiAu. The $T_N(P)$ phase boundary exhibits unconventional behavior in which the Néel temperature is enhanced from $T_N \approx 33$ K at ambient pressure to a maximum of $T_N \approx 35$ K occurring at $P \approx 5.5$ GPa. Upon a further increase in pressure, T_N is monotonically suppressed to ~22 K at $P \approx 27$ GPa. We also find a crossover in the temperature dependence of the electrical resistivity ρ in the antiferromagnetic (AFM) phase that is coincident with the peak in $T_N(P)$, such that the temperature dependence of $\rho = \rho_0 + A_n T^n$ changes from $n \approx 3$ during the enhancement of T_N to $n \approx 2$ during the suppression of T_N. Based on an extrapolation of the $T_N(P)$ data to a possible pressure-induced quantum critical point, we estimate the critical pressure to be $P_c \approx 45$ GPa.

DOI: 10.1103/PhysRevB.95.214403

I. INTRODUCTION

There are relatively few examples of materials that approximate a purely itinerant (or delocalized) electron magnet. Only the delocalized $3d$-electron bands of the transition-metal elements have the requisite energy bandwidth W and wave-vector magnitude k that can create a large density of states (DOS) at the Fermi energy ϵ_F that is unstable to the formation of a magnetically ordered ground state. The few transition-metal materials that approach the extreme case of pure itinerant-electron magnets include the weak itinerant ferromagnets (IFMs) $ZrZn_2$ [1] and Sc_3In [2] and the recently discovered weak itinerant antiferromagnet (IAFM) TiAu [3].

It is expected that significant effects are to be observed in the magnetic properties of weak IFMs under the application of pressure [4–6]. The application of pressure usually results in a reduction in magnetic order owing to a broadening of the electron bands and an associated decrease in the DOS(ϵ_F). This reduction in the DOS(ϵ_F) often dominates the expected increase in magnetization that results from an enhancement of the exchange interaction J as pressure is increased [6,7]. In the weak IFM $ZrZn_2$, the Curie temperature $T_C \approx 25$ K at ambient pressure is suppressed rapidly to $T_C = 0$ K toward a quantum critical point (QCP) at a modest critical pressure of $P_c = 0.85$ GPa [8–10]. However, it has been shown that the application of pressure can stabilize the band magnetism over a certain range of pressure, as observed in the anomalous behavior for the weak IFM Sc_3In, in which the magnetic ordering temperature is enhanced with the application of hydrostatic pressure up to $P \approx 3$ GPa [7,11].

In this report, we explore the effect of pressure on the Néel temperature T_N, in the IAFM TiAu, as a follow-up to the recent study on the suppression of T_N with chemical doping in the $Ti_{1-x}Sc_xAu$ system toward a QCP [12]. The initial report on the synthesis and characterization of polycrystalline samples of phase-pure, orthorhombic TiAu indicates that the intermetallic compound behaves as an IAFM with an ambient pressure Néel temperature $T_N = 36$ K [3]. Neutron diffraction measurements revealed a magnetic peak at the $\mathbf{Q} = (0,\pi/b,0)$ modulation vector well below T_N, with an estimated magnetic moment of 0.15 μ_B per formula unit [compared to the relatively large paramagnetic (PM) moment above T_N of $\mu_{PM} \simeq 0.8$ μ_B per formula unit, as derived from the linear fit of the high-temperature inverse susceptibility vs temperature]. In addition, muon spin relaxation (μSR) measurements revealed the existence of strong spin fluctuations in the PM phase above $T_N \simeq 35$ K, which quickly vanish throughout the sample volume over a small temperature range (~5 K) at the transition temperature [3].

Upon substitution of trivalent Sc^{3+} ions for Ti^{4+} ions, there is a rapid and monotonic suppression of the Néel temperature for the $Ti_{1-x}Sc_xAu$ system from $T_N = 36$ K at $x = 0$ toward a two-dimensional (2D) AFM QCP at a critical concentration of $x_c = 0.13$ [12]. The quantum phase transition to a two-dimensional antiferromagnet is reflected in both the linear temperature dependence of the electrical resistivity and the logarithmic divergence with decreasing temperature of the specific heat divided by temperature close to the QCP [12].

In the present study, the pressure dependence of T_N was determined from measurements of electrical resistivity ρ for several polycrystalline samples of TiAu as performed in various pressure cells over a range in pressure from $P = 0$ to 27 GPa. The features observed in the measurements of $\rho(T,P)$ allowed us to track the evolution of the Néel temperature T_N as

*Present address: Vacuum Process Engineering, Sacramento, California 95815, USA.
†Present address: Max Planck Institute for Chemical Physics of Solids, 01187 Dresden, Germany.
‡mbmaple@ucsd.edu

a function of pressure P. In contrast to the $T(x)$ dependence, we initially observe a positive pressure coefficient $dT_N/dP > 0$ at low pressure up to a maximum in T_N at $P \approx 5.5$ GPa, which is followed by a monotonic suppression of T_N with a further increase in pressure. The temperature dependence of the electrical resistivity was determined from power-law fits of the electrical resistivity $\rho = \rho_0 + A_n T^n$ to the $\rho(T)$ data above and below T_N. During the enhancement of T_N at low pressure ($P \leqslant 5.5$ GPa), $\rho(T)$ exhibits a T^3 temperature dependence in the antiferromagnetic phase. Interestingly, there is an abrupt change in the temperature dependence of $\rho(T)$ from T^3 to T^2 that is coincident with the peak in the $T_N(P)$ phase boundary at $P \approx 5.5$ GPa. As pressure is increased beyond 6 GPa and T_N is suppressed down to 22 K, $\rho(T)$ continues to exhibit a T^2 dependence up to $P \approx 25$ GPa. At this pressure, the anomalous drop in $\rho(T)$ is no longer detectable and $\rho(T)$ returns to a nearly T^3 behavior.

II. EXPERIMENTAL DETAILS

Polycrystalline samples of TiAu were prepared by arc melting Au and Ti as described previously in Ref. [3]. The measurements of electrical resistance R under pressure were performed for five different samples of TiAu in one of three types of pressure cells: (1) a piston cylinder cell (PCC), (2) a Bridgman anvil cell (BAC), and (3) a designer diamond anvil cell (DAC). The polycrystalline sample of TiAu (sample 0) measured in the PCC and the polycrystalline sample of TiAu (sample 1) measured in the first BAC are from the same synthesis performed at Rice University, while polycrystalline samples of TiAu (samples 2 and 3) measured simultaneously in the second BAC along with the polycrystalline sample of TiAu (sample 4) measured in the DAC are from a second synthesis performed at Rice University. While the geometrical factor for TiAu sample 0 measured in the PCC was easily determined, we note that the geometrical factor of the TiAu samples measured in the BACs and the DAC was too uncertain to yield a reasonable determination of the electrical resistivity ρ. Hence, we are only able to report the scaled electrical resistivity $\rho/\rho_{300\mathrm{K}}$ for the samples measured in the two BACs and the DAC, where $\rho_{300\mathrm{K}}$ is the value of electrical resistivity measured at 300 K.

In order to minimize the contact resistance for the sample measured in the PCC, a standard four-wire electrical resistivity measurement technique was used in which platinum wire leads were attached to the surface of the sample with two-part silver epoxy. The measurements of ρ in the PCC were performed at pressures ranging from ambient pressure ($P \approx 0$ GPa) up to a pressure $P \approx 1.8$ GPa in a one to one by volume mixture of n-pentane and isoamyl alcohol as a pressure-transmitting medium. The load was applied to the PCC at room temperature ($T \approx 300$ K), which is much higher than the melting point of the pressure-transmitting medium ($T \approx 120$ K) to ensure a nearly hydrostatic pressure environment. The pressure in the PCC at low temperature ($T < 4$ K) was determined by an inductive measurement of the superconducting transition temperature T_c of high-purity Sn (99.999%) and then compared with the established pressure dependence of T_c for Sn [13].

The measurements of electrical resistance R, for three different samples (TiAu samples 1, 2, and 3) in two different BACs were performed at pressures ranging from $P \approx 2.5$–16 GPa. TiAu sample 1 was measured independently in a BAC, and TiAu samples 2 and 3 were measured together in a second BAC. The pressure-dependent measurements of R in the BACs were made by using nonmagnetic tungsten carbide anvils to compress the sample in solid steatite used as a quasihydrostatic pressure-transmitting medium. Electrical resistance R was measured in a four-wire configuration in which electrical contact between the platinum leads and the surface of the TiAu samples was made by applying pressure with the tungsten carbide anvils. The pressure in the BAC was based on a four-wire electrical resistance measurement of T_c of a Pb sample placed inside the pressure cell which was compared with the established pressure dependence of the superconducting transition [$T_c(P)$] for Pb in the literature [13].

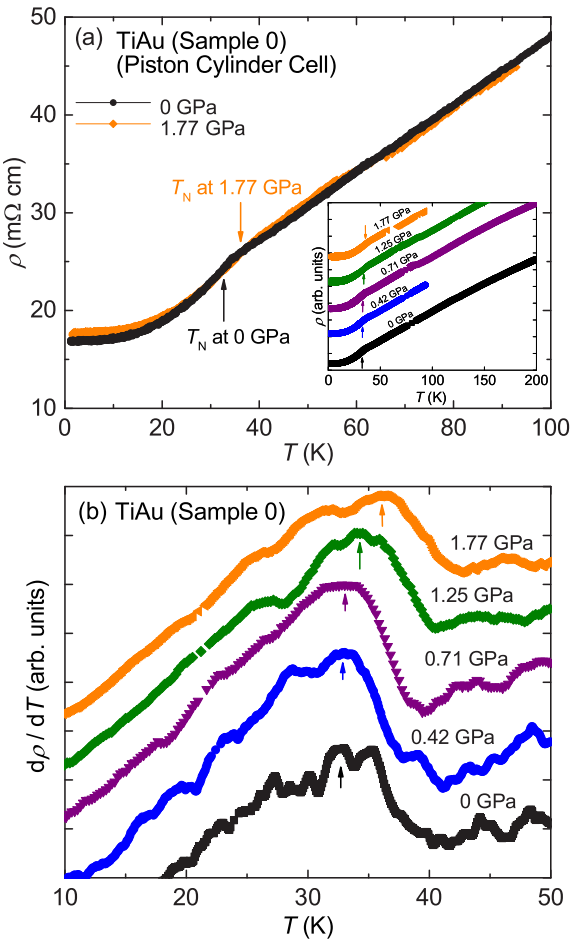

FIG. 1. (a) Electrical resistivity ρ vs temperature T at $P = 0$ and 1.8 GPa as measured in a piston cylinder cell (PCC). The arrows indicate the features in ρ that correspond to values of $T_N = 32.7$ K and 35.5 K at $P = 0$ and 1.77 GPa, respectively. Inset: Electrical resistivity ρ vs T up to $T = 200$ K at various pressures up to $P = 1.8$ GPa displaying the nearly linear temperature dependence and metallic behavior of ρ in the PM phase. The ρ vs T curves have been shifted vertically for clarity in illustrating the increase in T_N with increasing pressure. (b) The temperature derivative of the electrical resistivity $d\rho/dT$ vs temperature T at various pressures (shifted vertically for clarity). The Néel temperature at each pressure was determined from the maximum in $d\rho/dT$ as indicated by the arrows, and the values of T_N are listed in Table I.

The measurements of R in the designer diamond anvil cell were also performed using solid steatite as a quasihydrostatic pressure-transmitting medium for pressures ranging from $P \approx$ 2–27 GPa. The designer DAC consisted of a six-probe designer diamond anvil with a 250-μm culet that was paired with a standard diamond anvil with a slightly larger sized culet of 300 μm. A thin shard of polycrystalline TiAu was positioned on the culet of the six-probe designer diamond in order to make contact with the tungsten pads connected to the electrical probes. The sample space between the two culets, which contains the polycrystalline sample of TiAu, the solid steatite pressure-transmitting medium, and the ruby spheres used as manometers was sealed within a 100-μm hole that was drilled into the center of the indentation of a nonmagnetic gasket made of MP35N, an age-hardened nickel-cobalt base alloy [14]. The gasket was preindented to a thickness of $\sim$40 μm, and the hole was drilled into the gasket with an electric discharge machine (EDM). The pressure in the DAC was determined by tracking the shift in the R1 fluorescence line of the ruby spheres as pressure was increased at room temperature [15,16]. At low pressure, the R1 line was measured for two different ruby chips on opposing parts of the culet to rule out the presence of large gradients in pressure across the sample space. During the four-wire measurements of electrical resistance in each pressure cell, excitation currents were consistently set to be at 1 mA using an LR-700 Linear Research ac resistance bridge.

III. RESULTS AND DISCUSSION

A. Electrical resistivity measurements under pressure

The temperature dependence of the electrical resistivity $\rho(T)$ for TiAu as measured in the piston cylinder cell (PCC) at $P = 0$ and 1.8 GPa is shown in Fig. 1(a). At lower temperatures (for $T < 40$ K), there is a distinct feature or characteristic drop in the $\rho(T)$ data at T_N (as indicated by the vertical arrows), which is typical of a phase transition from a spin-disordered PM phase above T_N to a spin-ordered AFM phase below T_N. Typical metallic behavior with a positive temperature coefficient ($d\rho/dT > 0$) and a nearly linear temperature dependence is apparent in the $\rho(T)$ data for $T > 40$ K. Based on μSR measurements, the spin disorder in the PM phase is characterized by strong spin fluctuations that rapidly decay at the onset of the AFM order [3]. It is worth mentioning that in the IAFM TiAu, there is no gapping of the Fermi surface during the AFM transition. The abrupt decrease observed in the $\rho(T)$ data with decreasing temperature through T_N most likely reflects the disappearance of the short-range spin fluctuations during the phase transition from the PM phase to the AFM phase. This is in contrast to the anomalous jump in ρ, for example, as observed in elemental Cr just below $T_N \simeq 311$ K, at which point the formation of a gap over the Fermi surface results in a reduction in the carrier concentration and is associated with the emergence of an incommensurate long-range AFM spin fluctuation [17].

In order to illustrate the increase in T_N with increasing pressure, the $\rho(T)$ curves at various pressures up to $P = 1.8$ GPa have been shifted vertically for clarity, as shown in the inset of Fig. 1(a). Notice that the AFM ordering temperature increases monotonically with increasing pressure up to $P \approx 1.8$ GPa, as measured in the PCC such that $T_N = 32.7$, 32.9, 33.0, 34.2, and 35.5 K at $P = 0$, 0.42, 0.71, 1.25, and 1.77 GPa, respectively, at a rate of $dT_N/dP = 1.64$ K GPa^{-1}. As shown in Fig. 1(b), there are clear maxima observed in the the temperature derivative of the electrical resistivity $d\rho/dT$ at low pressures up to $P \approx 2$ GPa, and the values of the AFM ordering temperature T_N were easily resolved and determined from locating the maximum in $d\rho/dT$.

At ambient pressure, the shape of the peak in the $d\rho/dT$ vs T curve [black data at $P = 0$ GPa in Fig. 1(b)] is similar to the peak in the $d\rho/dT$ vs T previously reported in Ref. [3]. The maximum in the $d\rho/dT$ vs T curve at ambient pressure is reminiscent of the small peak at T_N observed in the specific heat (C_p/T vs T) also reported in Ref. [3]. Based on the analysis from previous studies of the specific heat curves for second-order transitions associated with (anti-)ferromagnetic materials [18,19], it is clear from the C_p/T vs T curve in Ref. [3] that a subtraction of the nonmagnetic contributions to the specific heat, i.e., the lattice and electronic contributions, would yield a magnetic contribution to the specific heat C_m, with a peak similar to that observed in the ambient pressure $d\rho/dT$ vs T curve. This correspondence between the peaklike curve of $d\rho/dT$ vs T and the peaklike behavior of the magnetic specific heat (represented by the shaded gray region in Fig. 2 of Ref. [3]) is consistent with a second-order phase transition in a system in which short-range spin fluctuations are the dominant contribution to the magnetic resistivity $\rho_{\rm mag}$ in an itinerant-electron system [20].

It is important to note that at low pressures ($P < 2$ GPa), the width of the peak in $d\rho/dT$ is already showing signs of broadening as pressure is increased. As discussed below, this

TABLE I. The values of the Néel temperature T_N, at pressure P, for the TiAu samples 0, 1, 2, 3, and 4 measured in the various pressure cells.

TiAu sample 0		TiAu sample 1		TiAu sample 2		TiAu sample 3		TiAu sample 4	
P (GPa)	T_N (K)	P (GPa)	T_N (K)	P (GPa)	T_N (K)	P (GPa)	T_N (K)	P (GPa)	T_N (K)
0	32.7	2.2	33.1	2.7	31.7	2.7	31.7	2.2	30.7
0.42	32.9	3.7	34.7	5.4	32.7	5.4	32.3	5.0	32.2
0.71	33.1	5.8	35.2	12.7	28.9	7.3	31.9	9.7	28.5
1.25	34.2	6.2	33.2	13.4	28.8	12.7	29.0	15.0	25.9
1.77	35.5			14.3	26.9	13.4	28.6	18.1	24.7
				14.8	26.8			26.7	22.1
				16.3	26.5				

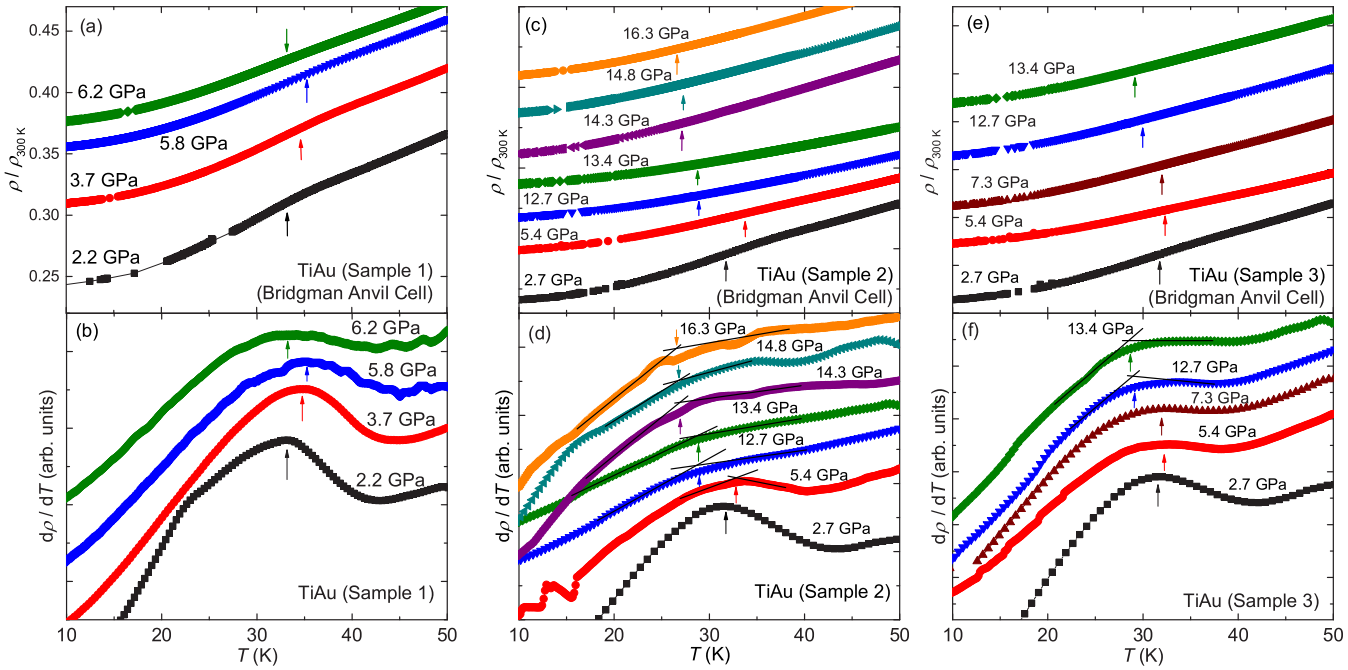

FIG. 2. Electrical resistivity $\rho/\rho_{300\mathrm{K}}$ (a,c,e) and its temperature derivative $d\rho/dT$ (b,d,f), as a function of temperature for three different polycrystalline samples of TiAu, as measured in a Bridgman anvil cell (BAC) at various values of pressure. The arrows indicate the feature at the AFM ordering temperature with the values of T_N extracted either from the maximum in $d\rho/dT$ or from the intersection of the linear extrapolations (solid black lines) of the $d\rho/dT$ vs T curves. The values of T_N at various P for TiAu samples 1, 2, and 3 measured in the two different Bridgman anvil cells are presented in Table I.

becomes problematic in determining the exact value of T_N at higher pressures above $P \approx 6$ GPa.

Figure 2 displays the temperature dependence of the electrical resistivity $\rho/\rho_{300\mathrm{K}}$ in the vicinity of T_N for three different polycrystalline samples of TiAu under pressure, as measured in two different BACs. The electrical resistance $R(T)$ for TiAu polycrystalline sample 1 was measured independently in a BAC up to $P \approx 6$ GPa and is displayed as $\rho/\rho_{300\mathrm{K}}$ in Fig. 2(a). The characteristic drop in ρ that occurs at T_N, as indicated by the vertical arrows, becomes less pronounced with increasing pressure. However, the values of T_N were easily determined from the location of the maxima in the temperature derivative of electrical resistivity ($d\rho/dT$), as shown in Fig. 2(b). The AFM ordering temperature is enhanced with increasing pressure from $T_N = 33.1$ K at $P = 2.2$ GPa up to a maximum of $T_N = 35.2$ K at $P = 5.8$ GPa at a rate of $dT_N/dP = 0.55$ K GPa^{-1}, after which there is a decline to $T_N = 33.1$ K at $P = 6.2$ GPa. It should be mentioned that for the $\rho(T)$ data at 2.2 GPa only, there are regions of missing data below 27 K. In order to generate the continuous temperature derivative of the electrical resistivity at 2.2 GPa ($d\rho/dT$ vs T), as shown in Fig. 2(b), some amount of interpolation and smoothing was required in performing the differentiation of the raw data. However, owing to the sufficient amount of data in the vicinity of $T_N = 33.1$ K, the effect of interpolation and smoothing on the location of the maximum $d\rho/dT$ were well within the error in determining T_N.

A similar trend in the behavior of T_N with increasing applied pressure is observed in the electrical resistivity $\rho/\rho_{300\mathrm{K}}$ for both polycrystalline TiAu samples 2 and 3, as displayed in Figs. 2(a) and 2(e), respectively. (TiAu samples 2 and 3 were measured simultaneously in a second BAC that was distinct from the BAC used to measure TiAu sample 1.) As observed in the case for TiAu sample 1, the characteristic drop in ρ at T_N (marked by the vertical arrows) is difficult to resolve in the $\rho(T)$ data at pressures above $P = 5$ GPa, as displayed in Figs. 2(c) and 2(e). When possible, the location of the maximum in $d\rho/dT$ was used to determine the value of T_N as marked by the arrows in the $d\rho/dT$ vs T plots [Figs. 2(d) and 2(f)]. Arrows indicating the location of T_N are also shown in the plots of $\rho/\rho_{300\mathrm{K}}$ vs T [Figs. 2(c) and 2(e)]. Clear maxima are observed in $d\rho/dT$ up to $P \approx 5.5$ and 7.5 GPa for samples 2 and 3, respectively, as shown in Figs. 2(d) and 2(f). However, at higher values of pressure, it was necessary to determine T_N from a different procedure by which T_N was defined to be the intersection of the linear extrapolations of the $d\rho/dT$ curves above and below T_N, as indicated by the black lines in Figs. 2(d) and 2(f). At $P = 2.7$ GPa, both TiAu samples 2 and 3 appear to undergo the transition into the AFM phase at $T_N = 31.7$ K. The ordering temperature increases with further application of pressure at a rate of $dT_N/dP = 0.30$ K GPa^{-1} to a maximum value of $T_N \approx 32.5$ K at $P \approx 5.5$ GPa.

The values of the AFM ordering temperature T_N are nearly identical for samples 2 and 3 up to $P = 13.4$ GPa. However, at lower pressures up to $P \approx 6$ GPa the values of T_N are somewhat smaller than the values of T_N that were observed for TiAu sample 1 measured in the BAC, which reaches a maximum of $T_N = 35.2$ K at $P = 5.8$ GPa. Nevertheless, the pressure dependence of T_N for all three samples measured in the two BACs is qualitatively consistent, in which T_N initially increases with pressure and passes through a maximum at $P \approx 5.5$. There is a large and monotonic suppression of the

AFM order with a further increase in applied pressure such that T_N is reduced to $T_N \approx 26$ K at $P \approx 16$ GPa. The suppression of AFM order can be seen in the shift of the intersection of the linear extrapolations (or "knee") in the $d\rho/dT$ vs T curves as shown in Figs. 2(d) and 2(f). [We mention that the absence of $\rho(T)$ data at higher pressures for sample 1 ($P > 6.2$ GPa) and sample 3 ($P > 13.4$ GPa) was due to failure of the electrical leads in the high-pressure Bridgman anvil cell.]

Measurements of electrical resistance under pressure $R(P,T)$ were extended to higher pressures up to $P \approx 27$ GPa with the use of a designer diamond anvil cell. The temperature dependence of the scaled electrical resistivity $\rho/\rho_{300\mathrm{K}}$ in the neighborhood of T_N at various pressures from $P = 2.2$–26.7 GPa are displayed in Fig. 3. The characteristic drop in ρ at the AFM transition at $T_N = 31.6$ K is just detectable in the $\rho(T)$ curves at $P = 2.2$ and 5.0 GPa; each of these $\rho(T)$ curves exhibits a clear maximum observed in their temperature derivatives ($d\rho/dT$), as shown in Fig. 3(b). The AFM ordering temperature for $P > 5.0$ GPa, as measured in the DAC, was defined to be the temperature at the intersection

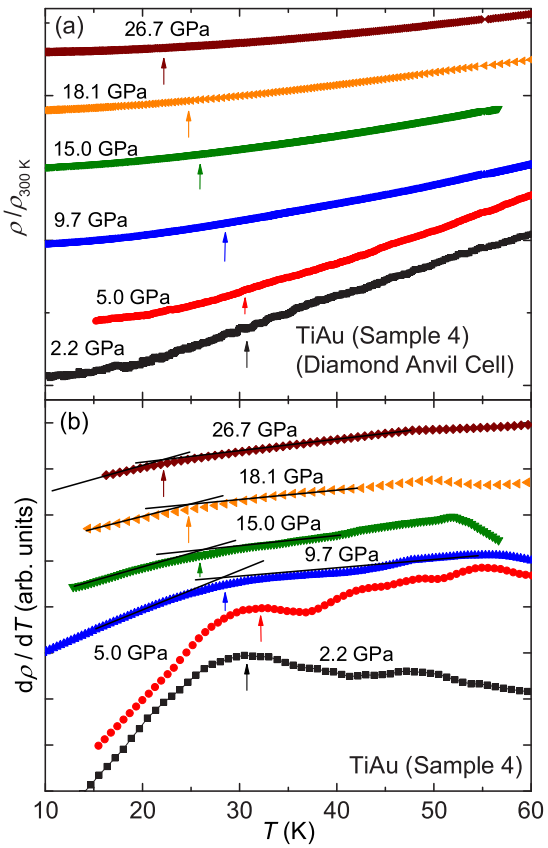

FIG. 3. (a) Electrical resistivity $\rho/\rho_{300\mathrm{K}}$ vs temperature T in the vicinity of the AFM ordering temperature T_N at various pressures up to $P \approx 27$ GPa as measured in a diamond anvil cell (DAC). The arrows point to the features at T_N. (b) Temperature derivative of the electrical resistivity $d\rho/dT$ vs T. The values of $T_N = 30.7$ and 32.2 K at $P = 2.2$ and 5.0 GPa, respectively, were determined from the maximum in the $d\rho/dT$ vs T curves, whereas the values of $T_N = 28.5$, 25.9, 24.7, and 22.1 K at $P = 9.7$, 15.0, 18.1, and 26.7 GPa, respectively, were determined from the intersection of the linear extrapolations (solid black lines) of the $d\rho/dT$ vs T curves as shown in panel (b).

of the linear extrapolations (solid black lines) of the $d\rho/dT$ curves above and below T_N, as shown in panel (b) of Fig. 3. (This method is similar to the determination of the values of T_N at higher pressures for TiAu samples 2 and 3.) The Néel temperature increases from $T_N = 30.7$ K at $P \approx 2.2$ GPa to 32.2 K at $P \approx 5.0$ GPa. As pressure is increased further, the AFM order is suppressed to $T_N = 22.1$ K at $P \approx 27$ GPa at a rate of approximately $dT_N/dP = -0.48\ \mathrm{K\ GPa^{-1}}$.

The temperature dependence of the electrical resistivity $\rho = \rho_0 + A_n T^n$, in the neighborhood of T_N, is displayed in Fig. 4 as a series of power-law fits to the $\rho(P,T)$ data for TiAu under pressure. The top eight panels in Fig. 4 are fits to the data in the AFM phase ($T < T_N$) at selected pressures from the various pressure cells, while the bottom eight panels are fits to the data in the PM phase ($T > T_N$). A nearly linear temperature dependence describes the data above T_N in the PM phase up to 60 K for $P < 5.4$ GPa and a slightly larger power-law exponent of $n = 1.4$–1.7 describes the $\rho(T)$ data in the PM phase at higher pressures for $P = 10$–27 GPa. Below the Néel temperature in the AFM phase ($5\ \mathrm{K} < T < T_N$), the $\rho(T)$ behavior is described by a much higher exponent of $n = 2.8$ for low pressures up to $P \approx 2$ GPa. As pressure is increased slightly, the value of the power-law exponent approaches $n \approx 2$ as the pressure approaches $P \approx 6$ GPa. The $n = 2$ dependence remains as pressure is increased up to $P \approx 25$ GPa. It is interesting to note that the clear crossover to a T^2 dependence in the AFM phase is coincident with the peak in the $T_N(P)$ phase boundary at $P \approx 5.5$ GPa. In the PM phase, the temperature dependence is somewhat stagnant, but perhaps showing a slight increase from a linear temperature dependence toward a $T^{1.5}$ dependence as pressure is increased and T_N is reduced. The onset of T^2 behavior during the suppression of T_N for $P > 6$ GPa suggests there may be a crossover to a Fermi-liquid ground state in this pressure range. However, these power-law exponents are also consistent with the behavior of local moment (and also itinerant) AFM metals near T_N, as described by self-consistent renormalization (SCR) theory, in which spin fluctuations account for most of the scattering that can lead to a $A_n T^n$ ($n \approx 2$) term in the power-law behavior of the electrical resistivity [21].

B. The effect of applied pressure on antiferromagnetic order in TiAu

As mentioned in the Introduction, it has recently been reported that chemical doping has the effect of suppressing the AFM order in the TiAu metal toward a two-dimensional AFM QCP [12]. Magnetization, specific heat, and electrical resistivity measurements at ambient pressure provide evidence for a continuous suppression of the AFM order in the $Ti_{1-x}Sc_xAu$ system as a function of x up to a critical concentration of $x_c = 0.13$, at which point the system appears to exhibit a continuous second-order quantum phase transition (QPT) [12]. The 2D AFM QCP in the $Ti_{1-x}Sc_xAu$ system is supported by the logarithmically divergent electronic specific heat coefficient $\gamma(T)$ and the linear ($n = 1$) temperature dependence of the electrical resistivity ($\rho = \rho_0 + A_n T^n$) in the vicinity of the QCP [12].

The pressure dependence of T_N as determined from the measurements of $\rho(T)$ for TiAu under pressure in the various

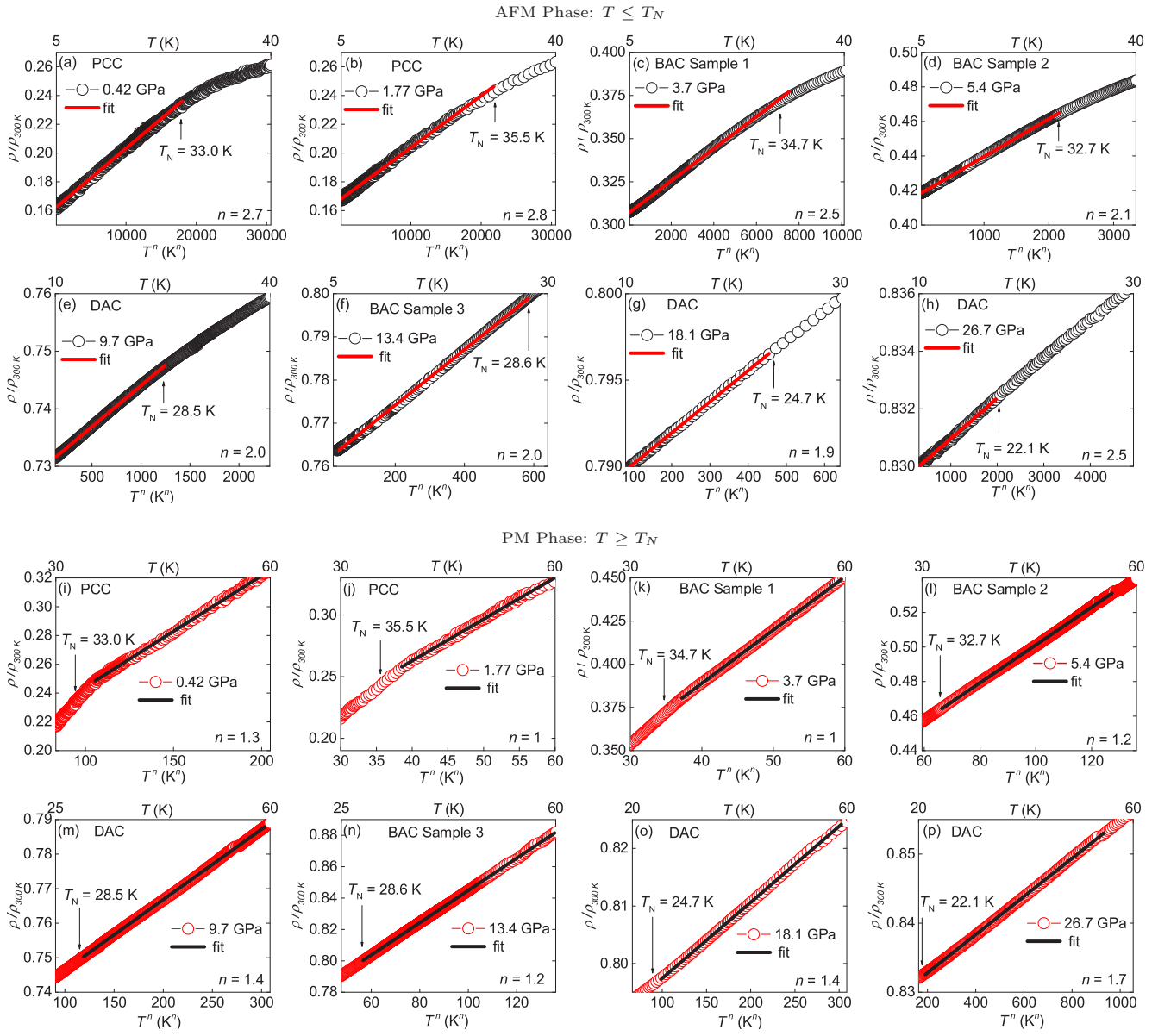

FIG. 4. Scaled electrical resistivity $\rho/\rho_{300\mathrm{K}}$ vs T^n above and below the Néel temperature T_N for TiAu under pressure P. Power-law fits of the electrical resistivity, $\rho = \rho_0 + A_n T^n$b to the $\rho(T)$ data were performed for $T < T_N$ in the AFM phase (top eight panels with black symbols and a red fit line) and for $T > T_N$ in the PM phase (bottom eight panels with red symbols and a black fit line). The upper x axis in each plot is shown as a linear T scale, and T_N is indicated by the black vertical arrows.

pressure cells is summarized in the T_N vs P phase diagram as shown in Fig. 5(a). There is a slight enhancement of AFM at low pressure. There is a clear peak in $T_N(P)$ boundary which is followed by a suppression of AFM as pressure is increased up to 27 GPa. (For comparison, the reader is referred to the T_N vs x phase diagram for the $Ti_{1-x}Sc_xAu$ system as reported in Ref. [12].) The values of T_N, as determined from measurements of ρ in the PCC, the two BACs, and the DAC, collectively indicate that the maximum in T_N occurs at $P \approx 5.5$ GPa. For pressures above $P \approx 6$ GPa, there is a monotonic suppression of the antiferromagnetic order. In particular, the Néel temperature is reduced to $T_N \approx 22$ K at a pressure of $P \approx 27$ GPa as measured in the DAC.

The evolution of T_N with P, in which there is an initial increase in T_N with pressure up to a maximum of ~35.5 K at $P \approx 5.5$ GPa, is distinct from the monotonic decrease in T_N observed with increasing x [12]. This contrasting behavior between the evolution of T_N with P and x in $Ti_{1-x}Sc_xAu$ is similar to what was observed for the IFM Sc_3In, in which the FM ordering temperature T_C is initially enhanced with increasing P but is monotonically suppressed toward a QCP with increasing x in $(Sc_{1-x}Lu_x)_{3.1}In$ [22]. In the $Ti_{1-x}Sc_xAu$ system, band-structure calculations reveal that the $3d$-electron bands of the Ti^{4+} ions contribute the most to the sharp peak observed in the DOS(ϵ_F) that leads to the magnetic ground state [12]. As x increases and more Sc^{3+} ions replace the

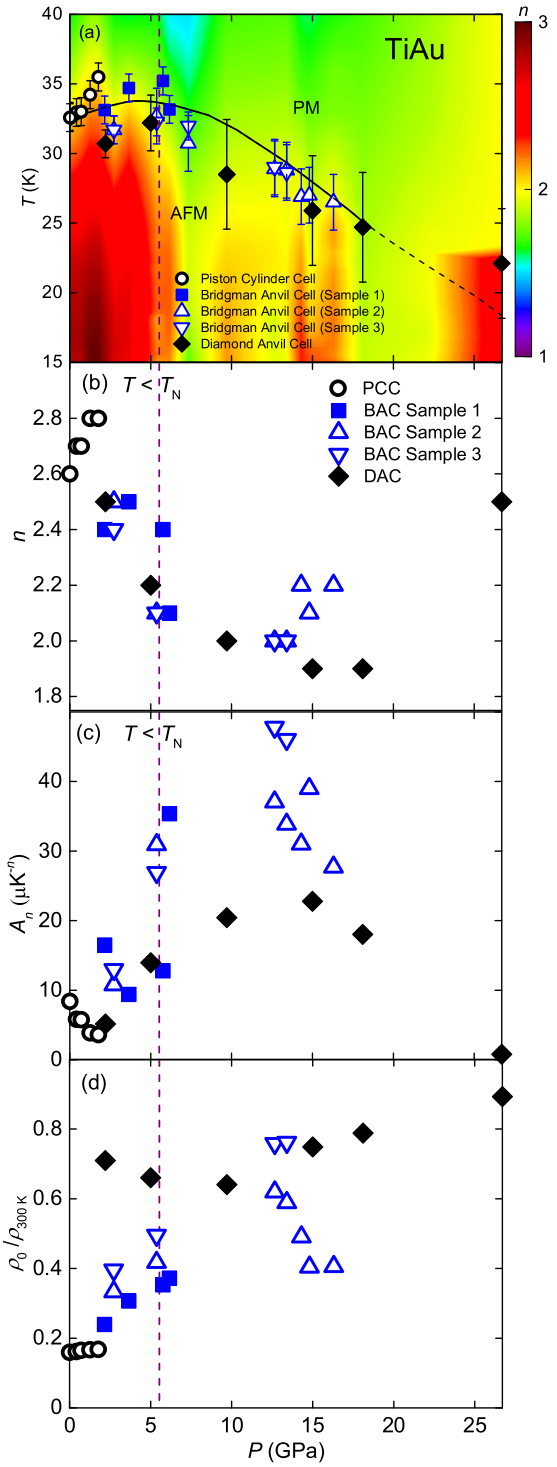

FIG. 5. (a) Temperature vs pressure (T_N vs P) phase diagram superimposed on a color contour representation of the exponent $n(P,T)$ from the electrical resistivity: $\rho = \rho_0 + A_n T^n$ (see text). The solid black curve is a guide to the eye and denotes the $T_N(P)$ phase boundary. (b,c,d) The parameters n, A_n, and ρ_0 vs pressure P were extracted from power-law fits of the electrical resistivity in the AFM phase as shown in Fig. 4. The dashed vertical line at $P = 5.5$ GPa is a guide to the crossover at the peak in $T_N(P)$.

Ti^{4+} ions, the peak in the DOS(ϵ) shifts away from the ϵ_F, leading to a reduction in the magnetic ordering temperature T_N [12].

On general grounds, the application of pressure should also lead to a suppression of the magnetic ordering temperature in an itinerant magnet in which the $3d$-electron bandwidth is broadened, leading to a decrease in the DOS at the Fermi level [7]. There are relatively few examples in the literature in which the application of pressure results in an enhancement of the magnetic ordering temperature [7,11,23–25]. In the case of the enhancement of FM order observed in the $Au_{1-x}V_x$ system, it was determined that there is an increase in the exchange interaction J as pressure is increased [25]. In the present study, there was no determination of the magnitude of J as a function of pressure. However, calculations of the band structure for TiAu under pressure indicate that the magnetic moment decreases monotonically with increasing pressure [26]. This suggests that the initial increase in T_N with pressure up to $P \approx 6$ GPa may result from an increase in J that is dominant over the decrease in the DOS(ϵ_F).

The distinct behavior observed in the evolution of T_N with increasing P in TiAu when compared with increasing x in the $Ti_{1-x}Sc_xAu$ system may result from the contrasting effects of pressure and doping on the unit-cell volume. There is an overall expansion of the unit-cell volume of TiAu by 4% upon substituting Ti with slightly larger Sc ions between $x = 0$ and 0.25 in $Ti_{1-x}Sc_xAu$. Most of the volume increase is due to the increase in the intraplanar lattice parameter b, while the interplanar spacing (lattice parameter c) remains unaffected with increasing Sc doping [12,26]. However, it is reasonable to assume that an application of pressure would result in a reduction of the unit-cell volume. In particular, under the most hydrostatic environment as observed in the PCC, the unit-cell volume of TiAu is more likely to contract isotropically, leading to conditions that might favor an enhancement of T_N, namely, an increase in the DOS at the Fermi level, or an enhanced exchange interaction J that could result from a contraction along the intraplanar (b) or interplanar (c) directions. Under a less hydrostatic environment, or as pressure is increased beyond a certain threshold value, the unit cell may contract or deform anisotropically, resulting in a monotonic decrease of T_N as suggested by calculations of the band structure under pressure [26]. In particular, a contraction solely along the interplanar c direction might result in a change to the relative unit-cell geometry, similar to the relative change observed upon Sc substitution in which there was an increase in the intraplanar lattice parameter b but no change in the interplanar spacing (lattice parameter c).

The T_N vs P phase diagram displayed in Fig. 5(a) is superimposed on a color contour representation of the power-law exponent $n(P,T)$ from the expression for the electrical resistivity: $\rho = \rho_0 + A_n T^n$. The representation of n was determined from the logarithmic derivative of the electrical resistivity $\partial \ln(\rho - \rho_0)/\partial \ln T$, which yields the local behavior of $n(P,T)$. Interestingly, the local behavior of $n(P,T) = \partial \ln(\rho - \rho_0)/\partial \ln T$ corroborates most of the values of T_N as determined from measurements of ρ (and the temperature derivatives, $d\rho/dT$) in the various pressure cells over the pressure range $P \approx 0$–27 GPa. This can be seen in the abrupt change in the value of n in the vicinity of T_N [i.e., at the $T_N(P)$ phase boundary]. The local change in $n(P,T)$ is most evident at lower pressures ($P \leqslant 6$ GPa) in which the power-law exponent changes abruptly from $n \approx 1.5$

(green-yellow) in the PM phase to $n \geqslant 2.5$ (yellow-red) in the AFM phase.

The effect of pressure on the parameters n, A_n, and ρ_0 (in the expression $\rho = \rho_0 + A_n T^n$) below the Néel temperature is summarized in Figs. 5(b), 5(c), and 5(d), respectively. At each pressure, the expression for ρ was fit to the $\rho(T)$ data in the AFM phase over the temperature range 5 K $< T <$ T_N. (Examples of power-law fits at selected pressures are displayed in Fig. 4.) The values of the power-law exponent n in Fig. 5(b) are consistent with the local behavior of $n(P,T)$ represented by the color contour in Fig. 5(a). The representations of n in panels (a) and (b) of Fig. 5 both show a clear crossover at $P \approx 6$ GPa from an $n \geqslant 2.5$ dependence during the enhancement of T_N to an $n = 2$ dependence during the suppression of T_N as pressure is increased above 6 GPa. Both the A_n coefficient and the residual electrical resistivity ρ_0 (at $T = 2$ K) increase steadily with increasing pressure up to $P \approx 15$ GPa, as shown in Figs. 5(b) and 5(c), respectively. While the residual electrical resistivity ρ_0 represents the contribution of impurity scattering to ρ, it is well recognized that spin fluctuations also play a significant role in the electrical resistivity of both ferromagnetic (FM) and AFM metals [21,27]. This is often reflected in the large value of the coefficient A_2 in the $A_2 T^2$ term [21,27]. Here, we observe that the coefficient A_n appears to strengthen with increasing pressure up to $P \approx 15$ GPa. It is interesting to note that A_n reaches a maximum as the temperature dependence of the electrical resistivity stabilizes toward T^2 behavior (where n reaches a minimum). However, it should be mentioned that the parameter n is naturally conflated with the parameter A_n, making it difficult to speculate on their relative role in scattering processes.

C. The effect of sample quality and nonhydrostatic pressure on the Néel temperature

The values of T_N determined for TiAu sample 0 measured in the PCC and TiAu sample 1 measured in the initial BAC are approximately 3 K higher than the values of T_N for TiAu samples 2 and 3 that were measured in the second BAC and TiAu sample 4 measured in the DAC. The samples in the PCC and the first BAC were from the same synthesis but different than the synthesis that yielded the two samples in the second BAC and the sample in the DAC. This may indicate that the nominal value of T_N at ambient pressure may be sensitive to varying conditions during synthesis. Figure 6 shows a plot of the Néel temperature T_N vs the residual resistivity ratio (RRR) at a pressure $P \approx 2$–3 GPa for the five different TiAu samples measured in this study. It is apparent that for RRR $\geqslant 3$, there is a significant increase in the Néel temperature from $T_N \approx 32$ K to $T_N \approx 35.5$ K. For RRR $\leqslant 3$, there is no significant change in T_N. In addition, the RRR values for the samples from the initial TiAu synthesis (namely, the PCC sample 0 and BAC sample 1) are 2–4 times larger than the RRR values for the samples from the second TiAu synthesis (namely, BAC samples 2 and 3 and the DAC sample 4).

Based on the $T_N(P)$ dependence observed in the various pressure cells, it appears that T_N is also sensitive to the degree to which the pressure environment is hydrostatic. There is a large response of T_N to pressure as performed in the PCC when compared to the response of T_N at low pressure as

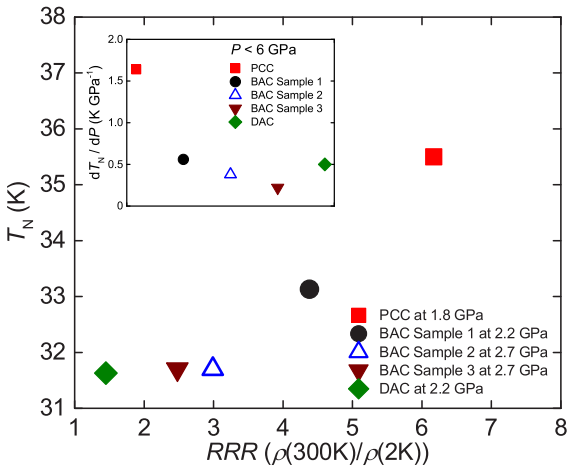

FIG. 6. A plot of the T_N vs residual resistivity ratio RRR = $\rho(300\text{ K})/\rho(2\text{ K})$ for the five TiAu samples measured in each of the various pressure cells at a low pressure of $P \approx 2$–3 GPa. Inset: Pressure coefficient dT_N/dP during the enhancement of T_N as pressure is increased up to $P \approx 6$ GPa for the five different TiAu samples.

performed in the two BACs and DAC. As shown in the inset of Fig. 6, the initial enhancement of T_N with P as observed in the PCC is $dT_N/dP = 1.64$ K GPa^{-1}, which is more than 3 times the enhancement of T_N with pressure as observed for the three samples measured in the two BACs and the sample measured in the DAC in which the pressure coefficients were observed to be $dT_N/dP = 0.56$ K GPa^{-1}, 0.38 K GPa^{-1}, 0.22 K GPa^{-1}, and 0.5 K GPa^{-1}, respectively. It is possible that the more hydrostatic conditions that are characteristic of the pressure-transmitting medium used in the PCC, when compared to the less hydrostatic environments typically achieved in the BAC and DAC, may result in the larger pressure coefficient, dT_N/dP, that we observed in the PCC up to $P \approx 2$ GPa. In previous investigations of the weak IFM Sc_3In, it was also found that the ferromagnetism is enhanced under the application of pressure under nearly hydrostatic conditions [7,11,28]. However, theoretical calculations show that the application of uniaxial strain (or nonhydrostatic pressure) results in a suppression of the magnetic order toward a possible QCP [30].

IV. SUMMARY

At temperatures below T_N, conduction electrons in local moment systems typically scatter from both long- and short-range spin fluctuations through the exchange interaction [21]. However, the long- and short-range fluctuations contribute differently to the electrical resistivity such that it is the short-range spin fluctuations that make the largest contribution to the electrical resistivity in a metal [20,21]. This scenario also applies to weak itinerant-electron systems such as TiAu in which the magnetic electrons are not localized [20]. Indeed, muon spin relaxation measurements [3] indicate that there is a rapid decay in the short-range spin fluctuations over a narrow temperature range during the transition from the PM phase to the AFM phase. This is reflected in the characteristic drop observed in the electrical resistivity $\rho(T)$ at T_N.

Recently, it was found that $T_N = 36$ K for the novel IAFM TiAu may be suppressed monotonically upon chemical doping toward a 2D AFM QCP [3,12]. This served as the motivation for the present study in which we investigated the response of the magnetic order to applied pressure in the IAFM TiAu. As previously mentioned, there is an inherent competition between the strengthening of the exchange interaction (that tends to increase T_N) and the reduction (or broadening) of the DOS at the Fermi level (that tends to reduce T_N) as pressure is increased. However, at sufficiently high pressure, it is expected that the broadening of the $3d$-electron bandwidth W is dominant over the increase in the exchange interaction, thus leading to a reduction in the magnetic ordering temperature (either T_C or T_N) [7].

In this investigation of the IAFM TiAu under pressure, we found that there is an initial enhancement of T_N with pressure up to $P \approx 6$ GPa, after which T_N is reduced monotonically to $T_N \approx 22$ K at $P \approx 27$ GPa. This is in contrast to the monotonic suppression of T_N with increasing Sc concentration x in the $Ti_{1-x}Sc_xAu$ system. Unfortunately, the characteristic drop in the electrical resistivity ρ is not well resolved at higher pressures, preventing a complete report on the suppression of T_N toward a QCP, as was observed in the chemical doping study for $Ti_{1-x}Sc_xAu$. The change in the temperature dependence of the electrical resistivity suggests there may be a crossover to a possible Fermi-liquid ground state in the AFM phase as T_N passes through its maximum value. We found that during the enhancement of T_N, the power-law behavior of the electrical resistivity follows an $n = 3$ dependence which switches to an $n = 2$ dependence as T_N is suppressed with a further increase in pressure up to $P \approx 27$ GPa. However, it should be mentioned that on the basis of SCR theory for itinerant AFM metals, spin fluctuations are the dominant scattering mechanism responsible for both an $n = 2$ temperature dependence and also a large coefficient in the A_2T^2 term [21]. In the AFM phase below $T = 30$ K, there was no change observed in the magnetization $M(H)$ at ambient pressure in high fields up to $H = 65$ T [26]. Further experiments involving simultaneous application of both field and pressure are suggested in order to better determine the nature of the magnetic state (and possible scattering mechanisms at play) in the various regions of the T_N vs P phase diagram, both before and after the peak at $P \approx 5.5$ GPa.

Figure 7 shows a fit (dashed curve) of the scaling function $T_N = T_{N(P=0)} \times (1 - P/P_c)^{\alpha}$ to the T_N(P) data obtained from the measurements of ρ in the various pressure cells. The ambient pressure value of the Néel temperature $T_{N(P=0)}$ was set to 36 K, while the estimated value for the critical pressure was determined from the fit to be $P_c = 45 \pm 11$ GPa and the value for the scaling exponent α was determined from the fit to be $\alpha = 0.65 \pm 0.20$. The slope of the curve near $T_N = 0$ K, as indicated by the solid black line, is $dT_N/dP \approx -2.5\ \mathrm{K\,GPa^{-1}}$ while the slope of the nearly linear T_N(P) data accumulated from the various pressure cells up to $P = 27$ GPa is $dT_N/dP = -0.59\ \mathrm{K\,GPa^{-1}}$. There is a large error in the estimated values of both P_c and α, which is most likely due to the lack of T_N(P) data at higher pressure. Nevertheless, these values for the critical scaling parameters as well as the relative slopes for the two linear regions described previously are consistent with other systems that were forced toward a QCP with the application of pressure [9,29]. We note that the projected value of the critical pressure, $P_c = 45$ GPa, is significantly smaller than the prediction of $P_c = 80$ GPa based on band-structure calculations [26]. The overestimation of P_c may result from the tendency of band-structure calculations to underestimate the role of electronic correlations. Hence, in the vicinity of a QCP, there is often an overestimation of the magnetic moment (or tendency towards magnetism), leading to an exaggerated value of P_c [30].

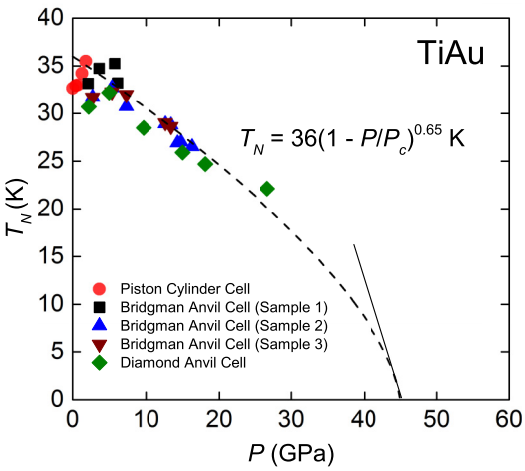

FIG. 7. (a) A temperature vs pressure (T_N vs P) phase diagram for TiAu showing the extrapolated $T_N(P)$ boundary (dashed curve) toward a critical pressure P_c at $T = 0$ K. The critical scaling function $T_N = T_{N(P=0)} \times (1 - P/P_c)^{\alpha}$ was fit to the T_N(P) data up to $P = 27$ GPa. The ambient pressure value of the Néel temperature ($T_{N(P=0)}$) was set to 36 K, while a rough estimate of the value for the critical pressure was determined from the fit to be $P_c = 45 \pm 11$ GPa. The value for the scaling exponent α was determined from the fit to be $\alpha = 0.65 \pm 0.20$. The slope of the curve near $T_N = 0$ K (represented by the solid black line) is $dT_N/dP \approx -2.5\ \mathrm{K\,GPa^{-1}}$, while the slope of the nearly linear T_N(P) data accumulated from the various pressure cells up to $P = 27$ GPa is $dT_N/dP = -0.59\ \mathrm{K\,GPa^{-1}}$.

ACKNOWLEDGMENTS

High-pressure research at the University of California, San Diego (C.W., Y.F., C.M., and M.B.M.) was supported by the National Nuclear Security Administration (NNSA) under the Stewardship Science Academic Alliance Program through the U.S. Department of Energy (DOE) under Grant No. DE-NA0002909. Low temperature measurements at UCSD were sponsored by the National Science Foundation (NSF) under Grant No. DMR 1206553. The work at Rice University (J.M.S., E.S., and E.M.) was supported by the NSF (DMR-1506704). High-pressure research at Lawrence Livermore National Laboratory (J.J., R.S., and S.W.) was partially supported by LDRD (Tracking Code 14-ERD-041) at Lawrence Livermore National Laboratory. Lawrence Livermore National Laboratory is operated by Lawrence Livermore National Security, LLC, for the U.S. DOE, NNSA under Contract No. DE-AC52-07NA27344. High-pressure research at the University of Alabama at Birmingham (Y.K.V) was supported by the U.S. DOE under Grant No. DE-NA0002928.

[1] B. T. Matthias and R. M. Bozorth, Ferromagnetism of a zirconium-zinc compound, Phys. Rev. **109**, 604 (1958).

[2] B. T. Matthias, A. M. Clogston, H. J. Williams, E. Corenzwit, and R. C. Sherwood, Ferromagnetism in Solid Solutions of Scandium and Indium, Phys. Rev. Lett. **7**, 7 (1961).

[3] E. Svanidze, J. K. Wang, T. Besara, L. Liu, Q. Huang, T. Siegrist, B. Frandsen, J. W. Lynn, A. H. Nevidomskyy, M. B. Gamza, M. C. Aronson, Y. J. Uemura, and E. Morosan, An itinerant antiferromagnetic metal without magnetic constituents, Nat. Commun. **6**, 7701 (2015).

[4] E. P. Wohlfarth, Forced magnetostriction in the band model of magnetism, J. Phys. C: Solid State Phys. **2**, 68 (1969).

[5] P. Mohn, Itinerant electron systems: Magnetism (ferromagnetism), in *Concise Encyclopedia of Magnetic and Superconducting Materials*, 2nd ed., edited by K. H. J Buschow (Elsevior Ltd., Amsterdam, 2005), pp. 340–351.

[6] J. S. Schilling, Some recent results in magnetism under high pressure, in *Physics of Solids Under High Pressure*, edited by J. S. Schilling and R. N. Shelton (North-Holland Publishing Company, Amsterdam, 1986), pp. 345–356.

[7] J. Grewe, J. S. Schilling, K. Ikeda, and K. A. Gschneidner, Anomalous behavior of the weak itinerant ferromagnet Sc_3In under hydrostatic pressure, Phys. Rev. B **40**, 9017 (1989).

[8] R. C. Wayne and L. R. Edwards, Effect of pressure on the Curie temperature of $ZrZn_2$, Phys. Rev. **188**, 1042 (1969).

[9] T. F. Smith, J. A. Mydosh, and E. P. Wohlfarth, Destruction of Ferromagnetism in $ZrZn_2$ at High Pressure, Phys. Rev. Lett. **27**, 1732 (1971).

[10] J. G. Huber, M. B. Maple, D. Wohlleben, and G. S. Knapp, Magnetic properties of $ZrZn_2$ under pressure, Solid State Commun. **16**, 211 (1975).

[11] W. E. Gardner, T. F. Smith, B. W. Howlett, C. W. Chu, and A. Sweedler, Magnetization measurements and pressure dependence of the Curie point of the phase Sc_3In, Phys. Rev. **166**, 577 (1968).

[12] E. Svanidze, T. Besara, J. K. Wang, D. Geiger, L. Prochaska, J. M. Santiago, J. W. Lynn, S. Paschen, T. Siegrist, and E. Morosan, Quantum critical point in the Sc-doped itinerant antiferromagnet TiAu, Phys. Rev. B (to be published).

[13] T. F. Smith, C. W. Chu, and M. B. Maple, Superconducting manometers for high pressure measurement at low temperature, Cryogenics **9**, 53 (1969).

[14] G. D. Smith, U.S. Patent No. 3,356,542.

[15] H. K. Mao, J. Xu, and P. M. Bell, Calibration of the ruby pressure gauge to 800 kbar under quasi-hydrostatic conditions, J. Geophys. Res. **91**, 4673 (1986).

[16] W. L. Vos and J. A. Schouten, On the temperature correction to the ruby pressure scale, J. Appl. Phys. **69**, 6744 (1991).

[17] E. Fawcett, Spin-density-wave antiferromagnetism in chromium, Rev. Mod. Phys. **60**, 209 (1988).

[18] J. A. Hofmann, A. Paskin, K. J. Tauer, and R. J. Weiss, Analysis of ferromagnetic and antiferro-magnetic second-order transitions, J. Phys. Chem. Solids **1**, 45 (1956).

[19] E. D. Thompson, Low temperature magnetic specific heat of nickel, Phys. Lett. **23**, 411 (1966).

[20] M. E. Fisher and J. S. Langer, Resistive Anomalies at Magnetic Critical Points, Phys. Rev. Lett. **20**, 665 (1968).

[21] Kazuo Ueda, Electrical resistivity of antiferromagnetic metals, J. Phys. Soc. Jpn. **43**, 1497 (1977).

[22] E. Svanidze, L. Liu, B. Frandsen, B. D. White, T. Besara, T. Goko, T. Medina, T. J. S. Munsie, G. M. Luke, D. Zheng, C. Q. Jin, T. Siegrist, M. B. Maple, Y. J. Uemura, and E. Morosan, Non-Fermi Liquid Behavior Close to a Quantum Critical Point in a Ferromagnetic State Without Local Moments, Phys. Rev. X **5**, 011026 (2015).

[23] T. F. Smith and W. E. Gardner, Pressure dependence of the superconducting transition temperature of uranium, Phys. Rev. **140**, A1620 (1965).

[24] W. E. Gardner and T. F. Smith, Superconductivity of α-uranium and uranium compounds at high pressure, Phys. Rev. **154**, 309 (1967).

[25] D. D. Jackson, J. R. Jeffries, W. Qiu, J. D. Griffith, S. McCall, C. Aracne, M. Fluss, M. B. Maple, S. T. Weir, and Y. K. Vohra, Structure-dependent ferromagnetism in Au_4V studied under high pressure, Phys. Rev. B **74**, 174401 (2006).

[26] E. Svanidze, Search, discovery, synthesis, and characterization of itinerant magnets composed of non-magnetic constituents, Ph.D. thesis, Rice University, 2015.

[27] T. Moriya, *Spin Fluctuations in Itinerant Electron Magnetism* (Springer-Verlag, Berlin, 1985).

[28] P. C. Riedi, J. G. M. Armitage, and R. G. Graham, Forced magnetostriction and pressure dependence of the magnetism of weakly ferromagnetic $Y(Co_{1-x})_2$ and Sc_3In, J. Appl. Phys. **69**, 5680 (1991).

[29] N. Kernavanois, S. Raymond, E. Ressouche, B. Grenier, J. Flouquet, and P. Lejay, Neutron diffraction study under pressure of the heavy-fermion compound $CePd_2Si_2$, Phys. Rev. B **71**, 064404 (2005).

[30] A. Aguayo and D. J. Singh, Itinerant ferromagnetism and quantum criticality in Sc_3In, Phys. Rev. B **66**, 020401(R) (2002); **67**, 139902(E) (2003).